JOURNAL OF PROPULSION AND POWER
Vol. 31, No. 5, September–October 2015

Supersonic Combustion and Flame Stabilization of Coflow Ethylene and Air with Splitter Plate

Liwei Zhang,* Jeong Yeol Choi,† and Vigor Yang‡
Georgia Institute of Technology, Atlanta, Georgia 30332

DOI: 10.2514/1.B35740

A numerical investigation of supersonic combustion for ethylene and air coflow with a splitter plate is presented, mimicking the flame stabilization and combustion establishment in a dual-combustion ramjet engine. Emphasis is placed on the detailed flow and flame characteristics immediately downstream of the splitter plate and in the shock-wave/shear-layer interaction regions. Three different splitter-plate thicknesses, 2, 4, and 8 mm, are considered, to identify the significance of the geometric parameters. The analysis is based on the Favre-averaged conservation equations for compressible chemically reacting flows. Turbulence closure is achieved using Menter's shear-stress transport model with a detached-eddy-simulation extension. Chemical reactions are modeled using a nine-species, ten-step laminar chemistry model with sufficient numerical resolution. Various mechanisms dictating the flame anchoring and spreading properties are examined. The hot stream from the ethylene preoxidization in the gas generator is found to behave like an underexpanded supersonic jet. Its subsequent expansion in the present wall-confined environment has a strong influence on the near-field mixing and combustion. Depending on the splitter-plate thickness, the wake region behind the splitter plate changes in size, and the autoignited flame can be either attached to or detached from the rim. The majority of chemical reactions take place in the mixing layer farther downstream, and the combustion efficiency varies in accordance with the near-field phenomena.

Downloaded by GEORGIA INST OF TECHNOLOGY on September 7, 2015 | http://arc.aiaa.org | DOI: 10.2514/1.B35740

Nomenclature

d	=	diameter of gas-generator exit nozzle, cm
M	=	Mach number
p	=	pressure, kPa
R_1	=	radius of gas-generator exit nozzle, cm
R_2	=	outer radius of isolator, cm
T	=	temperature, K
t	=	time, s
u, v	=	velocity components, m/s
x, r, z	=	spatial coordinates, m
Y	=	mass fraction
Z	=	mixture fraction
δ	=	thickness of splitter plate, mm
ρ	=	density, kg/m^3
ω	=	vorticity, s^{-1}

Subscripts

A	=	property of air
f	=	property of fuel
i	=	property of species i

I. Introduction

OVER the last two decades, there has been a renewed interest in scramjet engines as propulsion systems for high-speed air vehicles [1–3]. At hypersonic flight speeds of Mach 5.0 and above, the airflow must remain supersonic throughout the engine to avoid overheating and excessive pressure loss [4]. The ensuing flow residence time in the combustor chamber is typically on the order of milliseconds, within which the fuel must be injected, vaporized, mixed with air, and burned. In addition, the inlet flow is closely coupled with the combustor chamber dynamics and provides conditions conducive for driving flow and combustion instabilities. These limitations, combined with a low air static temperature, pose severe challenges for effective ignition and stable combustion, especially with heavy hydrocarbon fuels. Two leading design concepts have been developed and implemented to address these issues: the dual-mode scramjet (DMSJ) and the dual-combustor, also known as the dual-combustion, ramjet (DCR) engines [3]. In a DMSJ engine, combustion can occur at either subsonic or supersonic speed, or a combination of the two. In a DCR engine, a subsonic ramjet combustor precedes the main coaxial supersonic scramjet burner. The dump-type subsonic combustor, acting as a fuel-rich gas generator and a pilot flame, enables the use of conventional hydrocarbon fuels without resorting to logistically unsuitable additives [2,3].

The DCR concept was originally proposed by James Keirsey in the 1970s [2]. Billig et al. [5,6] and Waltrup [7] later extended the design for the development of integral-rocket dual-combustion ramjets. Figure 1 shows schematically an axisymmetric DCR engine. The featured shock structures are represented by single lines and clusters of lines. The incoming air, first compressed by the external compression surface, is divided by the inner cowl into two parts: a small fraction entering the inner duct connected to a subsonic combustor and the remaining portion passing over the cowl surface into the outer duct. An isolator prevents combustion-induced disturbances from interacting with the inlet flow. Depending on the operating conditions, the subsonic combustor burns either part or all of the fuel. It acts as a gas generator and a pilot flame. The hot products from the fuel-rich combustion are then injected into the main supersonic combustor for further reaction. As a result of reduced molecular sizes, enriched radicals, and elevated static temperature, the ignition capability and heat-release efficiency of this system are substantially higher than those with direct injection of heavy hydrocarbon fuels into supersonic flows [8,9]. In addition, the recirculating flow downstream of the rim of the subsonic combustor exit nozzle forms a low-speed, high-temperature region to assist flame anchoring. Self-sustaining combustion is thus achieved in the supersonic combustor without any additional flame-holding device. Although this concept was introduced and developed as many as 30 years ago, no thorough investigation of combustion establishment and flame stabilization has been performed to help identify the underlying physics and key design attributes.

Received 22 January 2015; revision received 30 March 2015; accepted for publication 6 April 2015; published online 8 June 2015. Copyright © 2015 by the authors. Published by the American Institute of Aeronautics and Astronautics, Inc., with permission. Copies of this paper may be made for personal or internal use, on condition that the copier pay the $10.00 per-copy fee to the Copyright Clearance Center, Inc., 222 Rosewood Drive, Danvers, MA 01923; include the code 1533-3876/15 and $10.00 in correspondence with the CCC.

*Research Engineer, School of Aerospace Engineering. Member AIAA.
†Visiting Professor. Member AIAA.
‡William R. T. Oakes Professor and Chair, School of Aerospace Engineering; vigor.yang@aerospace.gatech.edu. Fellow AIAA (Corresponding Author).

Downloaded by GEORGIA INST OF TECHNOLOGY on September 7, 2015 | http://arc.aiaa.org | DOI: 10.2514/1.B35740

The hot mixture from the subsonic combustor (referred to here as the gas generator) and the air from the isolator merge and react in the wake of the rim of the gas-generator exit nozzle (referred to here as the flame holder), in a configuration similar to a supersonic mixing layer with coflow fuel and air separated by a splitter plate. Most of the previous studies on supersonic mixing layers ignore the effect of the plate thickness [10–12], and a vast majority of theoretical studies of coflow diffusion flames assume infinitesimally thin splitter plates [13,14]. Only a few works take into account the influence of the finite thickness of the plate on the flow evolution. Clemens and Mungal [15] considered a splitter plate of 0.8 mm thickness, thinner than the boundary layer. A wake recirculation zone, nonetheless, was clearly observed downstream of the plate, followed by an expansion fan and an oblique shock. Yu et al. [16] found that the thickness of the splitter plate plays a decisive role in dictating the shear-layer evolution and large-scale vortices in the far field. Otakeyama et al. [17] experimentally examined the stability of CH_4/air jet diffusion flames with different rim thicknesses under subsonic flow conditions. The effect of splitter-plate thickness in supersonic coflow diffusion flames has not, however, been explored systematically.

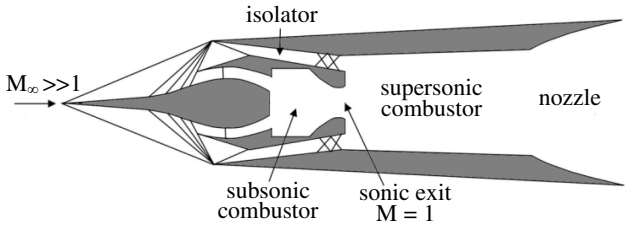

Fig. 1 Schematic of DCR engine with associated shock structures [5].

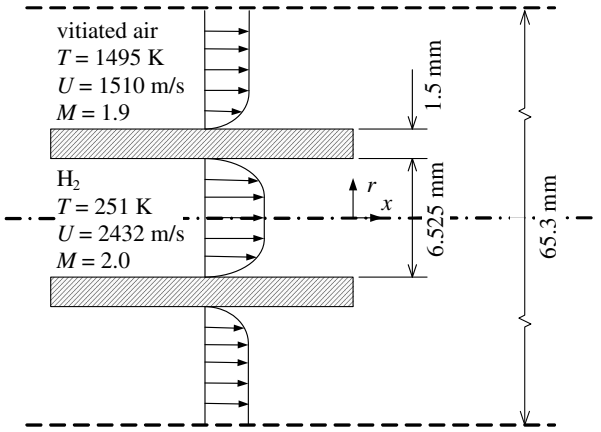

Fig. 2 Schematic of case 1 in [24].

Table 1 $C_2H_4 - O_2$ reaction system [22][a]

No.	Reaction	A_r	n_r	E_r
R1	$C_2H_2 + \Leftrightarrow 2CO + 2H_2$	1.80E + 14	0.0	35,500
R2	$CO + O \Leftrightarrow CO_2 + M$	5.30E + 13	0.0	−4, 540
R3	$CO + OH \Leftrightarrow CO_2 + H$	4.40E + 06	1.5	−740
R4	$H_2 + O_2 \Leftrightarrow OH + OH$	1.70E + 13	0.0	48,000
R5	$H + O_2 \Leftrightarrow OH + O$	2.60E + 14	0.0	16,800
R6	$OH + H_2 \Leftrightarrow H_2O + H$	2.20E + 13	0.0	5,150
R7	$O + H_2 \Leftrightarrow OH + H$	1.80E + 10	1.0	8,900
R8	$OH + OH \Leftrightarrow H_2O + O$	6.30E + 13	0.0	1,090
R9	$H + H \Leftrightarrow H_2 + H$	6.40E + 17	−1.0	0
R10	$H + OH \Leftrightarrow H_2O + M$	2.20E + 22	−2.0	0

[a]Units are in seconds, moles, cubic centimeters, calories, and Kelvin. The forward reaction rate constant k_{fr} for the rth reaction is $k_{fr} = A_r T^{n_r} \exp(E_r/RT)$.

The purpose of the present work is to investigate the flame stabilization and ensuing evolution of coflow ethylene and air in the wake of a splitter plate with finite thickness, mimicking the supersonic combustion in a DCR engine. Emphasis is placed on the near-field flow and flame development. The interaction with the resulting shock system is addressed in detail. The rest of the paper is organized as follows. Section II summarizes the theoretical formulation and numerical method for treating unsteady chemically reacting flows. Also included are the model validation and description of the flow geometry and operating conditions. Section III presents the results of both nonreacting and reacting cases. Conclusions are drawn in Sec. IV.

II. Theoretical Formulation and Numerical Method

The flow and flame dynamics are modeled using the Favre-averaged conservation equations of mass, momentum, energy, and species concentration for a multicomponent, chemically reacting system. Fick's law is used to approximate the species diffusion in a multicomponent mixture. Turbulence closure is achieved by

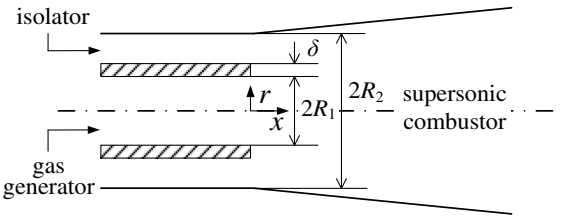

Fig. 4 Simplified configuration of DCR combustor.

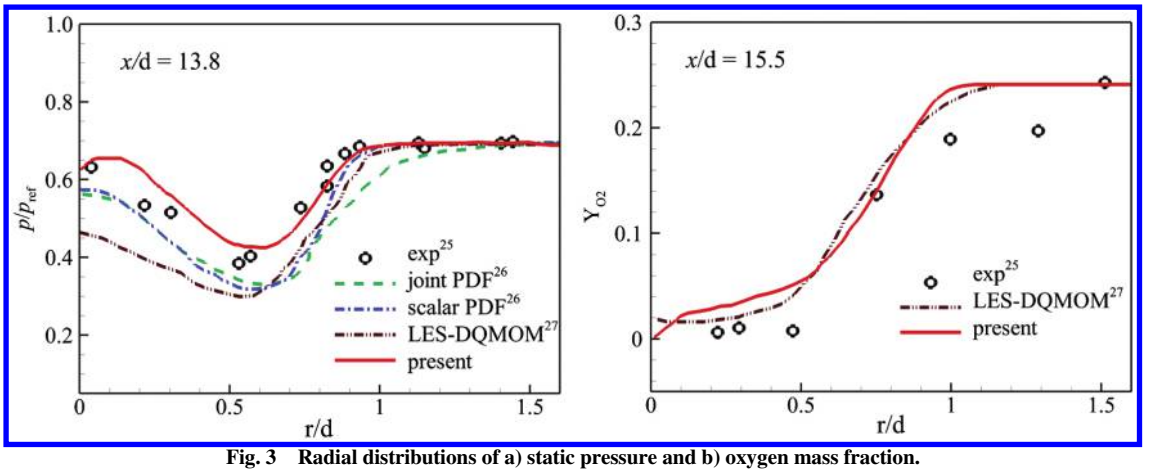

Fig. 3 Radial distributions of a) static pressure and b) oxygen mass fraction.

Downloaded by GEORGIA INST OF TECHNOLOGY on September 7, 2015 | http://arc.aiaa.org | DOI: 10.2514/1.B35740

Menter's shear-stress transport model augmented with a detached-eddy-simulation extension [18–20]. A detailed description of the theoretical formulation is given in [21].

A nine-species, ten-step kinetics scheme proposed by Singh and Jachimowski [22] is employed to treat the chemical reactions of ethylene and air, as shown in Table 1. This model was numerically assessed in a one-dimensional, steady-state, constant-density flowfield over a wide range of pressures, temperatures, and equivalence ratios. The results agreed well with those from a detailed 25-species, 77-reaction model that had been validated against experimental data [23]. Nitrogen is treated as an inert gas. Its effect appears in the evaluation of mixture composition and thermophysical properties.

The governing equations and associated boundary conditions are solved using a finite-volume approach. The convective fluxes are evaluated by means of Roe's flux-differencing splitting method derived for multispecies reacting flows. A third-order monotonic upstream-centered scheme for conservation laws is employed for extrapolations of primitive variables at the cell interface. This spatial discretization strategy satisfies the total-variation-diminishing condition and features a high-resolution shock-capturing capability. Temporal integration is achieved by a fully implicit, lower/upper symmetric Gauss–Seidel method. A Newton subiteration method is applied to reduce the error in the temporal discretization and ensure a second-order temporal accuracy and stability. The treatment allows for a time step corresponding to a Courant-Friederichs-Lewy number of 3.0 based on the minimum grid size. More details on the numerical procedure are available in [21]. The code is parallelized by a message-passing-interface technique to enhance computational efficiency.

A. Model Validation

The overall approach is validated against the experimental test case 1 of Evans et al. [24]. Figure 2 shows the physical model of concern and flow conditions. The airflow was preheated by burning with hydrogen and then replenished with oxygen to maintain an oxygen volume fraction equal to the ambient condition. Supersonic hydrogen was injected through a circular nozzle.

In the numerical formulation, no-slip conditions were enforced at the inner and outer surfaces of the nozzle. The interface between the airflow and its surrounding area was treated as slip boundaries, an approach also adopted in [25–27]. The flowfield was assumed to be axisymmetric, and only one-half of the domain in the radial direction was calculated. The grids in the air induction channel, hydrogen injection nozzle, and the downstream region were 101×121, 101×65, and 961×401, respectively.

Figure 3 compares the calculated distributions of the pressure and oxygen mass fraction with experimental measurements. Also included are results from other simulations [26,27]. The discrepancy near the centerline may be attributed to the lack of fluid transport under the axisymmetric assumption and model uncertainties, as well as the uncertainty in experimental data and the limitations of the turbulence model. The differences between the present study and those using the probability density function (PDF)-based turbulence-combustion models in [26,27] appear to be limited. DQMOM in Fig. 3 stands for the direct quadrature method of moments, an Eulerian approach introduced in [27]. The laminar chemistry is therefore used in the present work, in light of its numerical expediency.

B. Physical Domain and Boundary Conditions

Figure 4 shows the physical model considered in the present study, comprising an annular isolator, a cylindrical gas generator, and a coaxial supersonic combustor. The flowfield was assumed to be axisymmetric to reduce the computational burden. The origin of the coordinates was located at the center of the gas-generator exit plane. The incoming airflow was divided between the isolator and the gas generator by a splitter plate, simulating the situation in a DCR engine. Ethylene fuel was delivered into the gas generator, where the burning with air occurred. Fuel-rich reactants then entered into the supersonic combustor in the direction parallel to the centerline.

The computational domain spanned 0.15 m upstream into the isolator and 0.51 m downstream into the supersonic combustor. The radius of the gas generator R_1 was fixed at 2.54 cm. The effect of the splitter-plate thickness δ was studied by considering values of 2, 4, and 8 mm. To maintain the same isolator cross-sectional area and air mass flow rate, the width of the annular isolator was set to 2.11, 2.03, and 1.87 cm, respectively. The outer radii of the isolator R_2 were thus 4.85, 4.97, and 5.21 cm, respectively. A divergence angle of 3 deg, starting from $x = 0$, was applied to the supersonic combustor to prevent thermal choking.

The total temperature and pressure of the incoming airflow were set to 1181 K and 855 kPa, respectively, simulating a flight Mach number of 6 and altitude of 20 km. At the isolator entrance, the airflow had a Mach number of 2.2, a temperature of 600 K, and a pressure of 80 kPa. The total pressure in the gas generator assumed a

Table 2 Species mass fractions at chemical equilibrium in the gas generator

	N_2	CO	H_2	H	H_2O	C_2H_4	CO_2	OH	O	O_2
Mass fraction	6.37×10^{1}	3.39×10^{-1}	2.43×10^{-2}	3.90×10^{-5}	1.38×10^{-5}	1.29×10^{-5}	6.67×10^{-6}	5.55×10^{-9}	1.15×10^{-11}	6.24×10^{-16}

Table 3 Flow conditions in simulation

	Isolator entrance (upper stream)	Gas-generator exit (lower stream)	
		Nonreacting flow	*Reacting flow*
Total temperature, K	1180	1180	2153
Total pressure, kPa	855	684	684
Static temperature, K	600	984	1794
Static pressure, kPa	80	362	362
Mach number	2.2	1.0	1.0

Table 4 Numerical grid matrices

			Supersonic combustor			
	Isolator	Gas generator	$\delta = 2$ mm	$\delta = 4$ mm	$\delta = 8$ mm	Total cell number
Level 1	100×50	50×50	— —	650×120	— —	8.55×10^4
Level 2	200×100	100×100	— —	1300×240	— —	3.42×10^5
Level 3	400×200	200×200	2600×440	2600×480	2600×560	1.37×10^6
Level 4	800×400	400×400	— —	5200×960	— —	5.47×10^6

Downloaded by GEORGIA INST OF TECHNOLOGY on September 7, 2015 | http://arc.aiaa.org | DOI: 10.2514/1.B35740

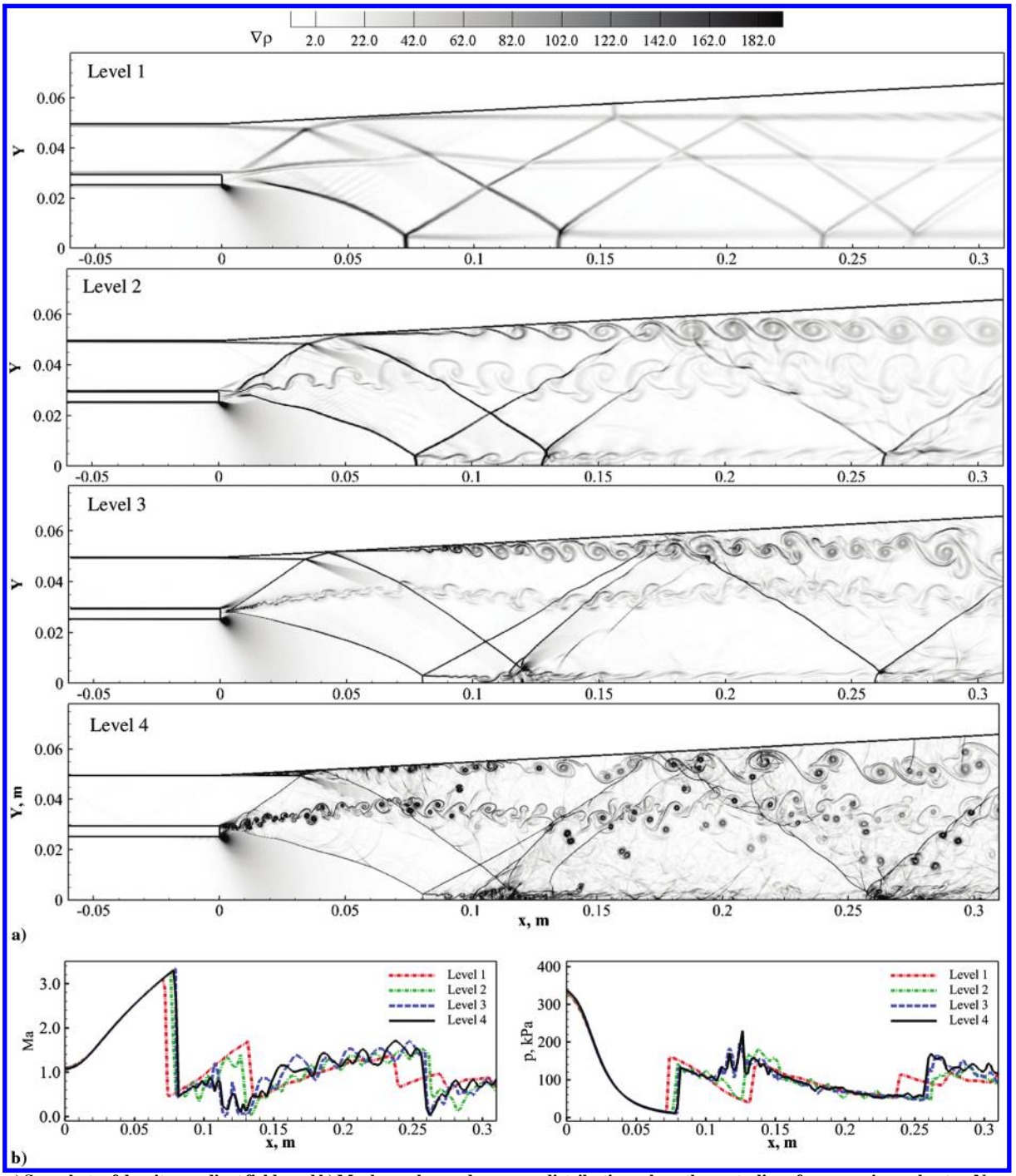

Fig. 5 a) Snapshots of density-gradient fields and b) Mach number and pressure distributions along the centerline of supersonic combustor. Nonreacting case with a splitter-plate thickness of 4 mm at four different grid resolutions.

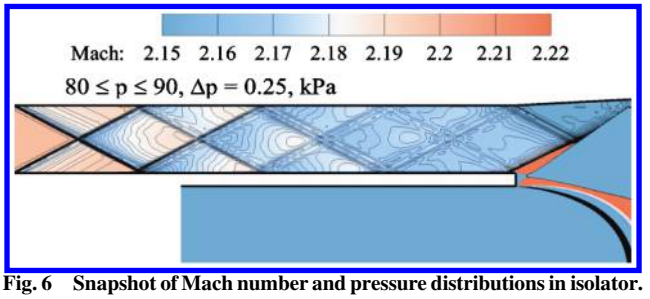

Fig. 6 Snapshot of Mach number and pressure distributions in isolator. Nonreacting case with a splitter-plate thickness of 4 mm.

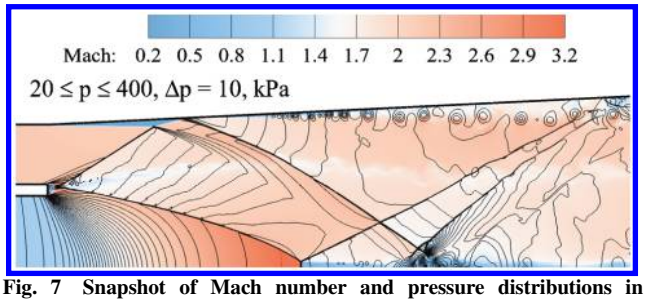

Fig. 7 Snapshot of Mach number and pressure distributions in combustor. Nonreacting case with a splitter-plate thickness of 4 mm.

value of 684 kPa. The static pressure and temperature at the choked gas-generator exit were 362 kPa and 984 K, respectively.

It is assumed that 75% of the air entered into the isolator, with the remaining 25% into the gas generator. If the overall fuel/air equivalence ratio took a nominal value of 0.75 for the engine, then the equivalence ratio in the gas generator became 3.0. Under such a fuel-rich condition, oxidation of ethylene was primarily attributed to the first reaction R1 in Table 1, mainly producing CO and H_2 along with limited amounts of C_2H_4, H, OH, O, H_2O, CO_2, and O_2. Table 2 lists the species mass fractions at the chemical equilibrium condition in the gas generator. The flame temperature was 2153 K, and the temperature at the choked nozzle exit was 1794 K. Table 3 summarizes the flow conditions in the present study for both nonreacting and reacting cases.

Boundary conditions were specified according to the method of characteristics. At the isolator and gas-generator entrances, the pressure and temperature were fixed at the aforementioned values. Broadband fluctuations with a turbulence intensity of 0.01 were supplemented to the isolator inflow. The gas-generator exit was

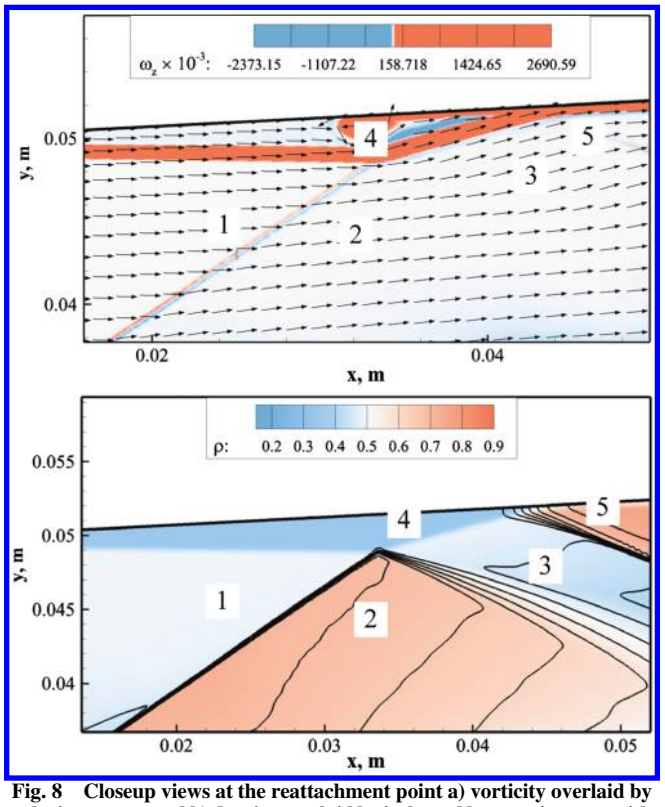

Fig. 8 Closeup views at the reattachment point a) vorticity overlaid by velocity vectors and b) density overlaid by isobars. Nonreacting case with a splitter-plate thickness of 4 mm.

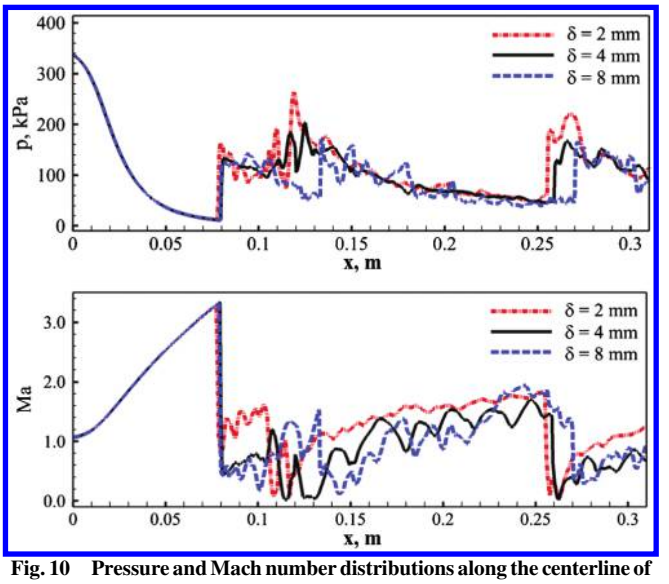

Fig. 10 Pressure and Mach number distributions along the centerline of supersonic combustor.

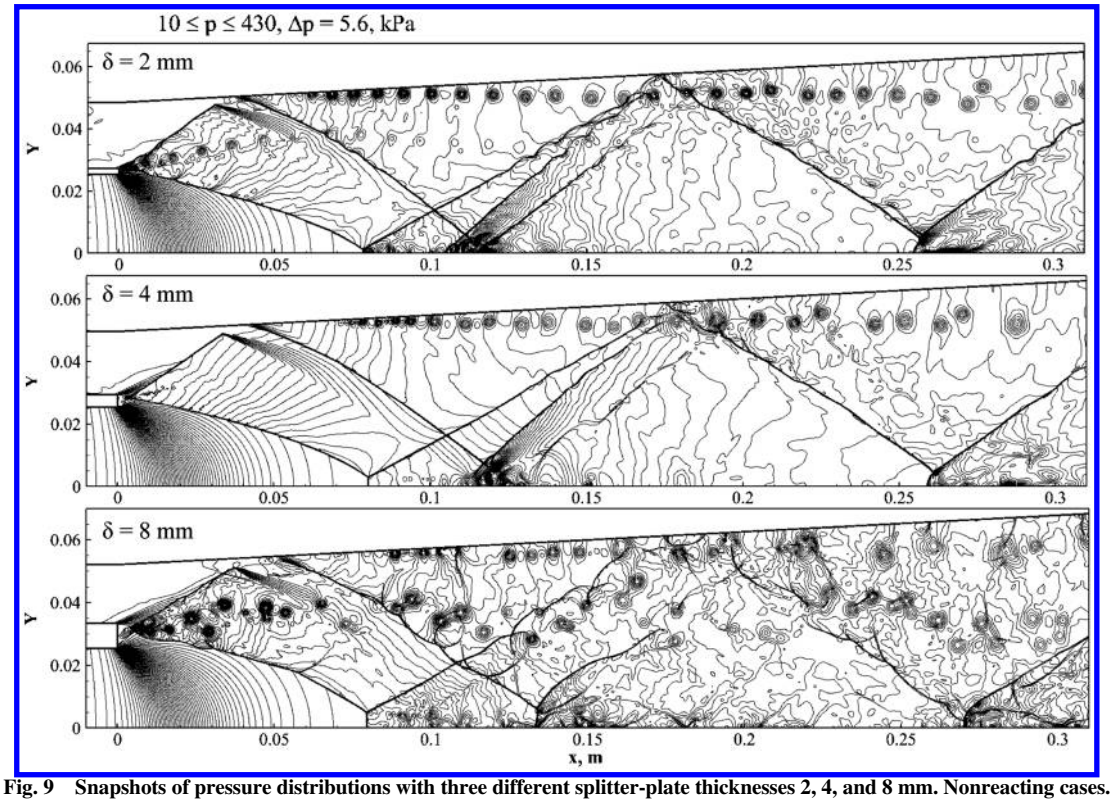

Fig. 9 Snapshots of pressure distributions with three different splitter-plate thicknesses 2, 4, and 8 mm. Nonreacting cases.

Downloaded by GEORGIA INST OF TECHNOLOGY on September 7, 2015 | http://arc.aiaa.org | DOI: 10.2514/1.B35740

Downloaded by GEORGIA INST OF TECHNOLOGY on September 7, 2015 | http://arc.aiaa.org | DOI: 10.2514/1.B35740

choked, and a fixed mass flow rate was enforced. At the exit of the computational domain, the flow was predominantly supersonic. Flow properties were extrapolated from interior points. Adiabatic and nonslip conditions were implemented along the solid walls, with the velocity and the normal gradients of other flow variables set to zero. Flow symmetry was applied at the centerline.

III. Results and Discussion

A. Nonreacting Flows

The nonreacting case was first studied to establish a fundamental understanding of the flow characteristics. To minimize numerical uncertainty, a grid-convergence study was performed with a splitter-plate thickness of 4 mm. Four different grid levels were considered, with a refinement ratio of 2 in each coordinate. Table 4 summarizes the numbers of finite-volume cells in the isolator, gas generator, and supersonic combustor, respectively. Note that for a different splitter-plate thickness the grid number in the radial direction was adjusted accordingly to ensure the same near-field resolution. The grid points were clustered toward walls to resolve stiff flow gradients in those regions. The numerical cells were evenly distributed radially in the wake of the splitter plate, with spatial resolution of 200, 100, 50, and 25 μm, respectively, for the four cases. The entire numerical domain was divided into 71 blocks to facilitate parallel computation.

Calculations were initiated by delivering the airflow through the isolator and gas generator at prespecified conditions at $t = 0$. The flowfield reached its stationary state after the initial transient at $t = 3.2$ ms. Figure 5a shows the instantaneous density-gradient fields at $t = 6.0$ ms for the four different levels of numerical resolution. The overall shock structures for levels 2–4 were generally similar, but their locations converged only for levels 3 and 4. Vortical structures became more distinguishable with grid refinement. At level 1, the shear layers appeared to be blurred, and limited details were visible. At level 2, the shear layers rolled up into wavy structures and further deformed under the influence of shock waves and turbulent dissipation. At level 3, fine structures in the shear layers were resolved, and their interactions with shock waves were clearly identified. At level 4, for which the numerical turnaround time was about ten times greater than that of level 3, considerable detailed information was captured. In summary, level 1 failed to provide key flow physics in spite of its ability to resolve shock waves. Levels 2 and 3 led to reasonable results at moderate computational costs. Level 4 had the potential to show detailed flow instabilities and their interactions with turbulence, at the expense of daunting computing resource requirements. Figure 5b shows the Mach number and pressure distributions along the combustor centerline. Numerical convergence was observed as the grids were refined. Results with level 3 resolution bore strong similarity to those with level 4. For the present study, the intermediate grid level 3 was employed, as a compromise between numerical burden and flow details.

1. *Flow Characteristics in Annular Isolator*

The isolator is a crucial component of a hypersonic propulsion engine. It ensures stable operation of the engine by protecting the inlet flow from disturbances arising in the combustor. Figure 6 shows the pressure and Mach number distributions in the annular isolator. The pressure increment is 0.25 kPa in the range of 80–90 kPa. The clustering of the isobaric lines marks the presence of shock discontinuities. Oblique shocks were formed by the reflection of the leading shocks issued from the isolator entrance. The shock waves were gradually dissipated in the downstream region, with a pressure decrease of less than 10 kPa through the isolator. The Mach number varied from 2.15 to 2.25 throughout the isolator. Immediately downstream of the splitter plate, intensive flow expansion occurred. The Mach number increased rapidly, and the pressure dropped sharply. It should be noted that the results will be quite different for the reacting case, as heat release in the combustor may cause severe flow blockage. The resultant flow separation near the isolator wall will detrimentally modify shock structures and flow characteristics [28,29].

2. *Flow Characteristics in Supersonic Combustor*

Figure 7 shows the instantaneous pressure and Mach number distributions in the near field of the splitter plate. The pressure increment is 10.0 kPa in the range of 20–400 kPa. The Mach number

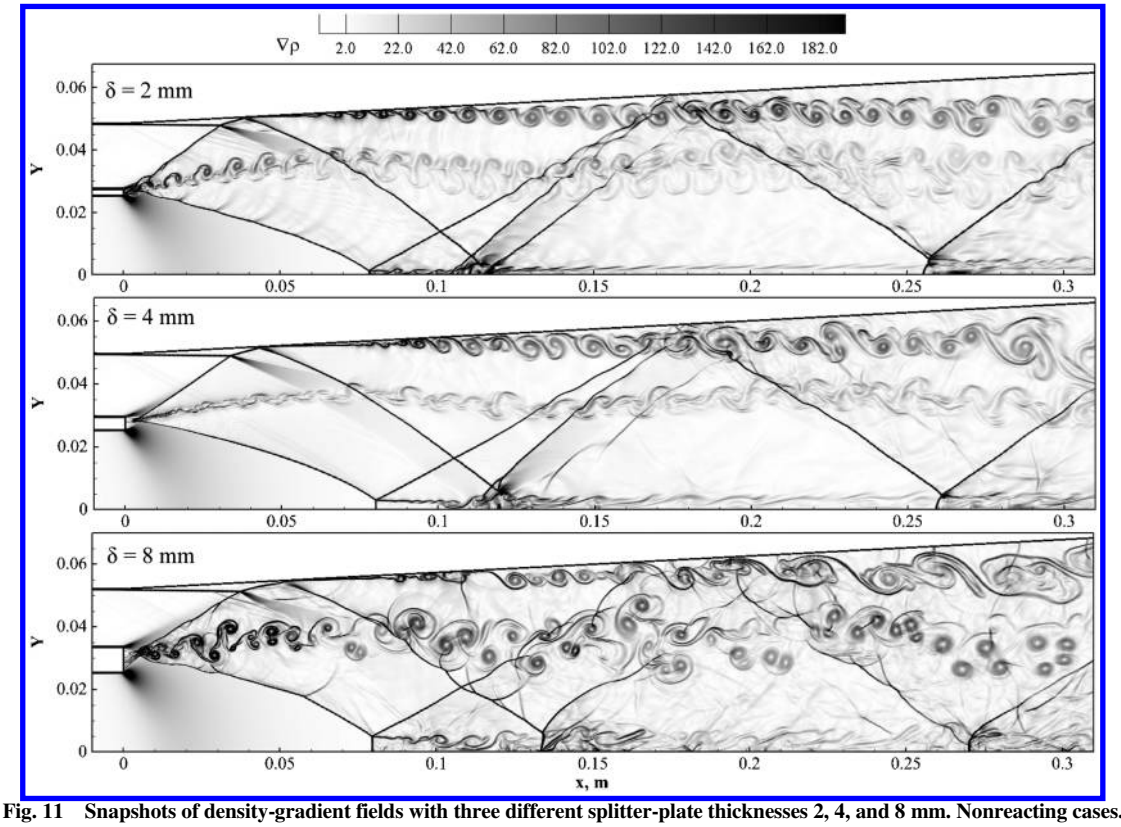

Fig. 11 Snapshots of density-gradient fields with three different splitter-plate thicknesses 2, 4, and 8 mm. Nonreacting cases.

Downloaded by GEORGIA INST OF TECHNOLOGY on September 7, 2015 | http://arc.aiaa.org | DOI: 10.2514/1.B35740

is colored between 0.2 and 3.2. Expansion waves stemming from the edges of the splitter plate were clearly observed. Flow separation occurred at the diverging point of the combustor wall ($x = 0$). Since the pressure changed modestly from the isolator to the combustor, expansion waves emanating from the upper edge of the splitter plate were indistinct in this color scale. In contrast, a well-established semi-oval expansion zone appeared at the lower edge of the splitter plate. As the flow passed through this region, its pressure dropped to below 80 kPa, and the Mach number rose above 3.0. Overexpansion occurred immediately downstream of the splitter plate, and a conical oblique shock formed to adjust the flowfield to match the isolator flow. The resultant barrel shock then reflected at a Mach disk (a strong shock normal to the flow direction) near the centerline, generating oblique shocks and Mach reflections in the far field. An oblique shock also appeared at the splitter-plate outer edge. It was incident to the separated shear layer near the wall and led to an expansion fan. The separated flow then reattached to the wall, forming a recirculation bubble and inducing another oblique shock near the reattachment point.

Figure 8 shows closeup views of the density and vorticity fields near the reattachment point, with isobars and velocity vectors, respectively. The shear layer separating the near-wall, low-density region and the main stream is marked by a red strip of positive vorticity, an indication of counterclockwise motion. The incident shock is manifested by a narrow zone featuring a stiff vorticity gradient. As the flow in zone 1 passed the oblique shock, it was compressed and diverted to the shock direction in zone 2. As soon as the shear layer met the incident shock, it bent toward and eventually reattached to the wall. The incident shock was reflected into an expansion fan, separating zones 2 and 3. The density and velocity mismatches between zones 3 and 4 led to the formation of a contact discontinuity indicated by a vorticity layer between the two zones. The flow in zone 3 was overexpanded. Another oblique shock formed near the attachment point, and the near-wall vorticity rolled up into a secondary shear layer in zone 5, as shown in Fig. 7.

3. *Effect of Splitter-Plate Thickness*

Figure 9 shows snapshots of the pressure field with three different splitter-plate thicknesses of 2, 4, and 8 mm. The pressure is in the range of 10–430 kPa with an increment of 5.6 kPa. As the splitter-plate thickness increased, the incidence location of the outer oblique shock on the combustor wall was delayed, the region enclosed by the inner oblique shocks expands, and the size of the first Mach disk increased. Figure 10 shows the pressure and Mach number distributions along the centerline of the combustor. The expansion zone is marked by a smooth rise in the Mach number and a gradual drop in pressure from $x = 0$ to 0.08 cm. Results with different splitter-plate thicknesses converge in this region. The distance between the gas-generator nozzle exit and the first Mach disk H_M can be estimated by an empirical correlation [30] as a function of the ratio of the nozzle stagnation pressure p_{tot} to the effective backpressure $p_{b,\text{eff}}$,

$$\frac{H_M}{d} = 0.67\sqrt{\frac{P_{\text{tot}}}{P_{b,\text{eff}}}}$$

where d is the diameter of the exit nozzle. In the current cases, d is 5.08 cm, and p_{tot} and $p_{b,\text{eff}}$ are 684 and 115 kPa, respectively. H_M is estimated to be 0.08 m, which matches the simulations well. As the splitter plate thickens, the size of the expansion zone increased, and the incidence angle of the barrel shock decreased, leading to a larger first Mach disk. Since the downstream flowfield was adjusted by shocks and contact discontinuities, the locations of the second and subsequent Mach disks varied among the three plots; the discrepancy exceeded 0.01 m in the third. Overall, the case with a splitter-plate thickness of 2 mm had the highest bulk Mach number and the shortest interval between two consecutive shock reflections.

Figure 11 compares the density-gradient distributions with different splitter-plate thicknesses. The primary mixing layer started immediately downstream of the splitter plate, between the outer and the inner oblique shocks. It grew laterally, intersected with and was diverted by shock waves, and diffused into the mainstream. The incident shock waves were reflected from either the combustor wall or the Mach disk. Secondary shear layers were generated by the shock-wave/shear-layer interactions. Combined, these discontinuities had significant impacts on the flow and flame dynamics. An effective resolution of these structures was necessary for a thorough examination of the mixing and combustion process. As the splitter plate thickens, the shear layers expanded, and their interactions with shocks were intensified, creating broader low-speed, high-temperature regions.

Of the subsonic zones, the one in the wake of the splitter plate was most important. Figure 12 shows the vorticity distributions and velocity vectors in the near field. As the flow passed the splitter plate, sudden expansion took place and led to boundary-layer separation. The separated flows with negative vorticity (clockwise motion) from the isolator and positive vorticity (counterclockwise motions) from the gas generator ran toward each other and merged at an axial distance of around 1.5, 2.2, and 3 mm, respectively, for the three splitter-plate thicknesses. Recirculating flows were created upstream of these intersection points, and mixing layers formed downstream. The behaviors of flow expansion varied with the splitter-plate thickness as follows. First, the upper and the lower recirculating

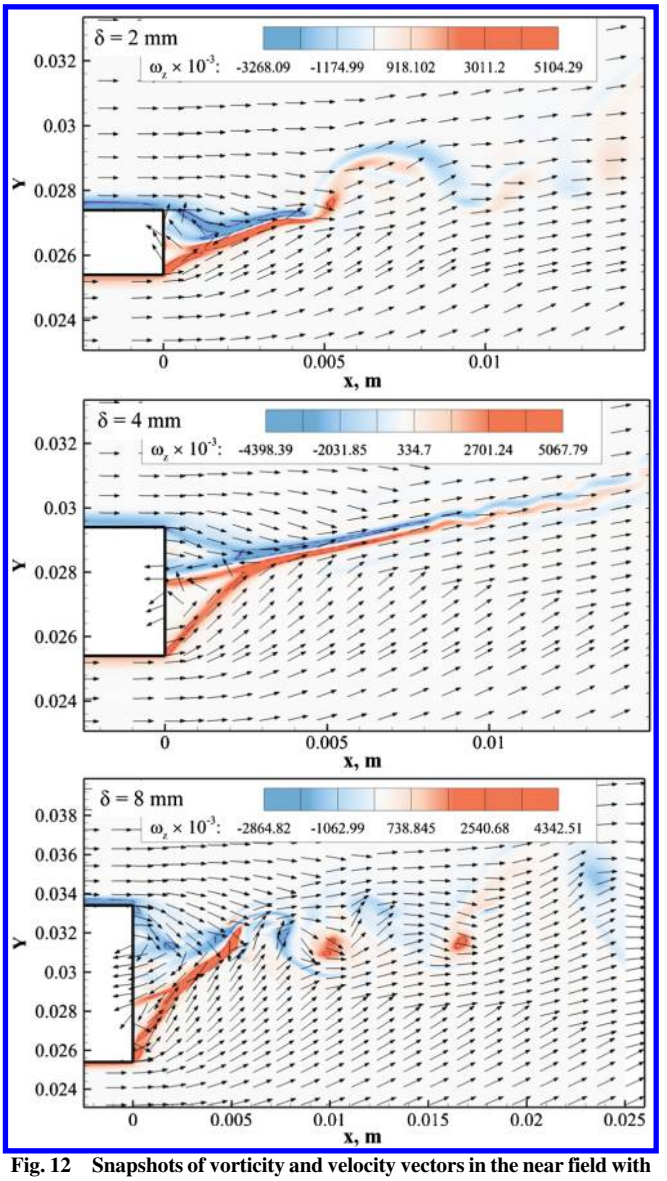

Fig. 12 Snapshots of vorticity and velocity vectors in the near field with three different splitter-plate thicknesses 2, 4, and 8 mm. Nonreacting cases.

zones merged for the 2 mm plate, made contact behind the 4 mm plate, and separated downstream of the 8 mm plate. Second, the vorticity was stratified in the 2 and 4 mm cases. In contrast, the stratification broke down in the 8 mm case at an axial distance of around 5 mm. These differences could have strong effects on the near-field mixing and ignition.

B. Reacting Flows

Once a fully developed nonreacting flowfield was achieved, oxidation of ethylene was activated in the gas generator. Products from the fuel-rich combustion were injected into the supersonic combustor. Data were collected after the initial transient was complete and the flowfield had reached its stationary state.

1. Flow and Flame Characteristics in Combustor

For comparison purposes, a supplemental case with ethylene oxidation in the gas generator but with frozen chemistry in the supersonic combustor was treated for a splitter-plate thickness of 4 mm. It was referred to as the semireacting case hereafter. Figure 13 shows snapshots of the temperature field in the semireacting case T_1 and the reacting case T_2 at the same time instant. As the gas-generator products entered the main combustor, the temperature T_1 immediately downstream of the splitter plate rose to above 1000 K, as shown in Fig. 13a. Autoignition thus occurred, and no external stimulus was required. As compared to Fig. 13a, the fully reacting case T_2 in Fig. 13b gained a bulk increase from chemical heat release. Note that the ethylene/air combustion had an adiabatic flame

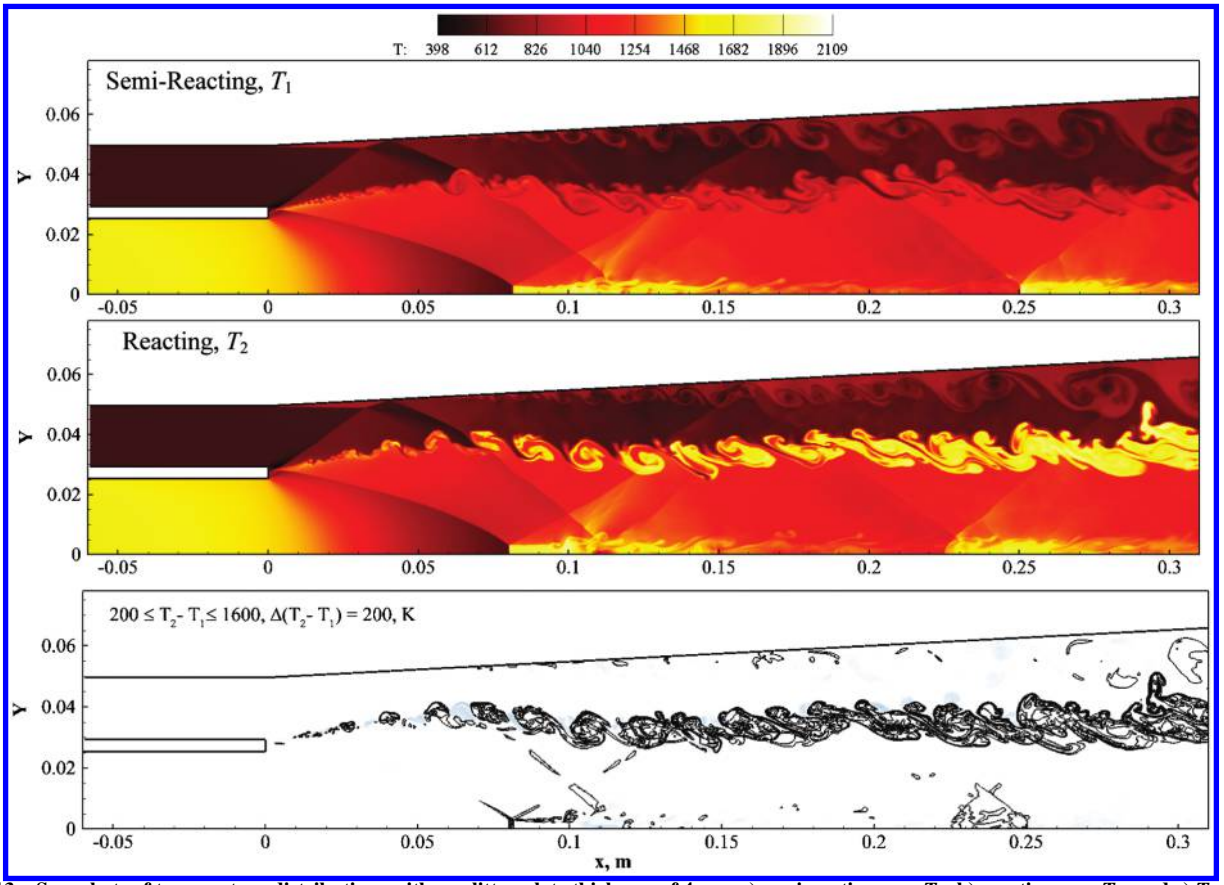

Fig. 13 Snapshots of temperature distributions with a splitter-plate thickness of 4 mm a) semireacting case T_1, b) reacting case T_2, and c) $T_2 - T_1$.

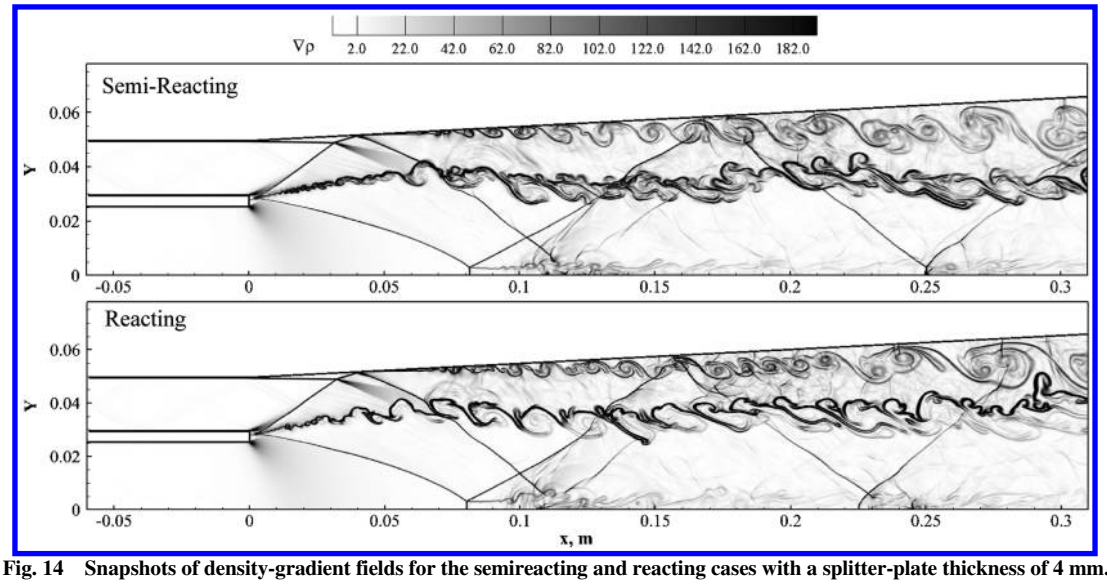

Fig. 14 Snapshots of density-gradient fields for the semireacting and reacting cases with a splitter-plate thickness of 4 mm.

Downloaded by GEORGIA INST OF TECHNOLOGY on September 7, 2015 | http://arc.aiaa.org | DOI: 10.2514/1.B35740

temperature of 2369 K at stoichiometric conditions and 1 atm. With T_2 exceeding 2100 K in moderately large zones and excessive air herein, it is believed that combustion was fully established in the current calculation.

Figure 13c shows the difference between T_1 and T_2. Negative values colored in blue indicate flow unsteadiness. Positive values are marked by isolines in the range of 200–1600 K at an increment of 200 K. The value of $T_2 - T_1$ represents reaction intensity and varies rapidly in the narrow zones across the mixing layer. The localized heat release affected flow structures and vice versa. Figure 14 shows the corresponding density-gradient contours. The shock system resembles its nonreacting counterpart in Fig. 11, albeit with slight upstream shifts of reflection locations. The overall unsteadiness in the shear layers was suppressed as a result of the increased viscosity at an elevated temperature, especially on the fuel side. The combustion-induced thermodynamic changes were manifold: 1) Viscous layers grew near reaction zones and hindered flow entrainment. 2) As the transport coefficients increased, fuel and oxygen were supplied to the reactions faster provided with proper scalar concentrations. 3) Because of local density decrease, the flowfield was more sensitive to incident instabilities, as suggested by a wavier near-field shear layer in the reacting case.

Figure 15 shows instantaneous distributions of the pressure, Mach number, vorticity, and mixture fraction. Large pressure variations mark the locations of shock waves. Heat release in the mixing layer drove the local flow evolution toward the sonic state. Vorticity production was enabled by shock-induced baroclinic torques. The ensuing intensive motions in the radial direction enhanced flow entrainment and promoted shear-layer transient, from a hydrodynamic instability induced small-scale sinusoidal motion to the large-scale fluctuations. To trace reactants in the current nonpremixed combustion, the mixture fraction was calculated as the total element fraction of C and H normalized by the amount initially in the gas-generator stream. Only values in the range of 0.1–0.9 are shown. Since the gas generator had a total ethylene/air equivalence ratio of 3.0, the mixture fracture herein corresponded roughly to an equivalence ratio of 0.3–2.7. The value is commonly considered to be within the ethylene/air flammability limit. Note that there were strong correlations between the temperature increase in Fig. 13c and the mixture-fraction distribution in Fig. 15, suggesting that mixing plays a critical role in dictating chemical reactions.

Analyses of reacting flows were further performed with splitter-plate thicknesses of 2 and 8 mm with the other conditions unchanged. Figures 16 and 17 present distributions of the temperature and CO_2 mass fraction for three different thicknesses, respectively. For the 2 mm case, the overall flow unsteadiness was relatively weak, with a concentrated mixing layer, especially in the far field after shock penetrations. As a result, the flame was restricted to a thin region, indicating low combustion efficiency and robustness. For the 8 mm case, the mixing layer was much fuller, with a higher bulk temper-

Downloaded by GEORGIA INST OF TECHNOLOGY on September 7, 2015 | http://arc.aiaa.org | DOI: 10.2514/1.B35740

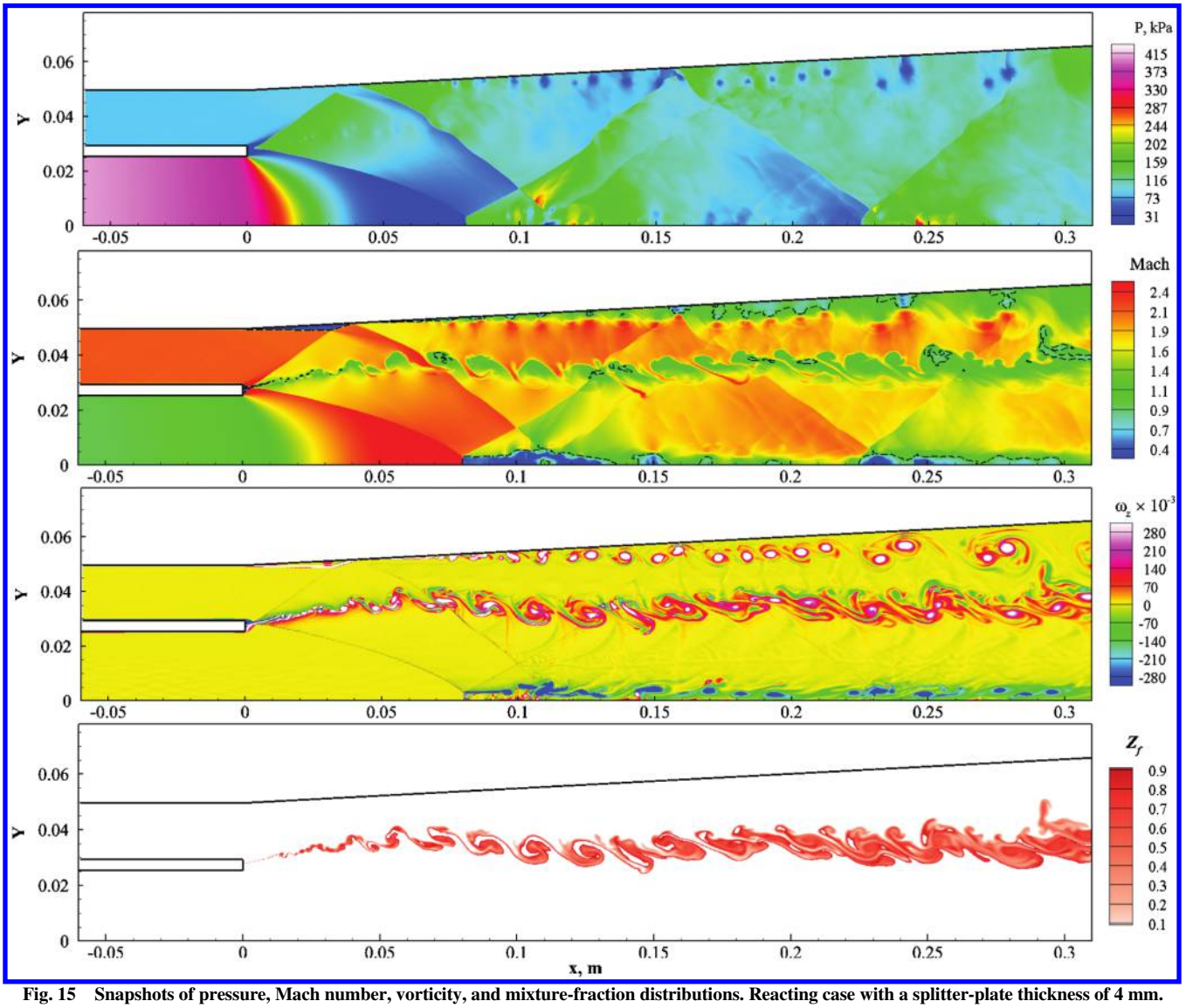

Fig. 15 Snapshots of pressure, Mach number, vorticity, and mixture-fraction distributions. Reacting case with a splitter-plate thickness of 4 mm.

Downloaded by GEORGIA INST OF TECHNOLOGY on September 7, 2015 | http://arc.aiaa.org | DOI: 10.2514/1.B35740

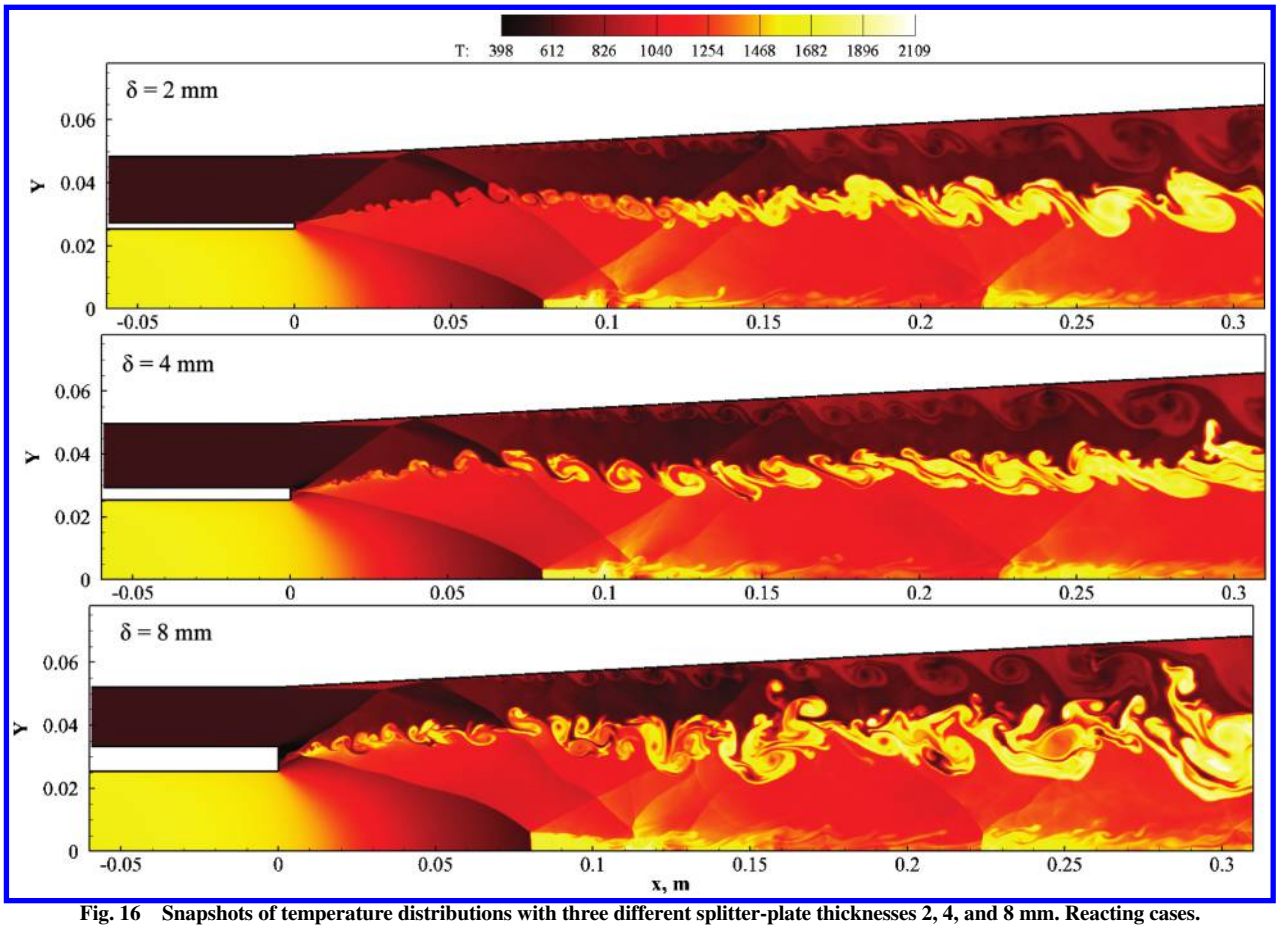

Fig. 16 Snapshots of temperature distributions with three different splitter-plate thicknesses 2, 4, and 8 mm. Reacting cases.

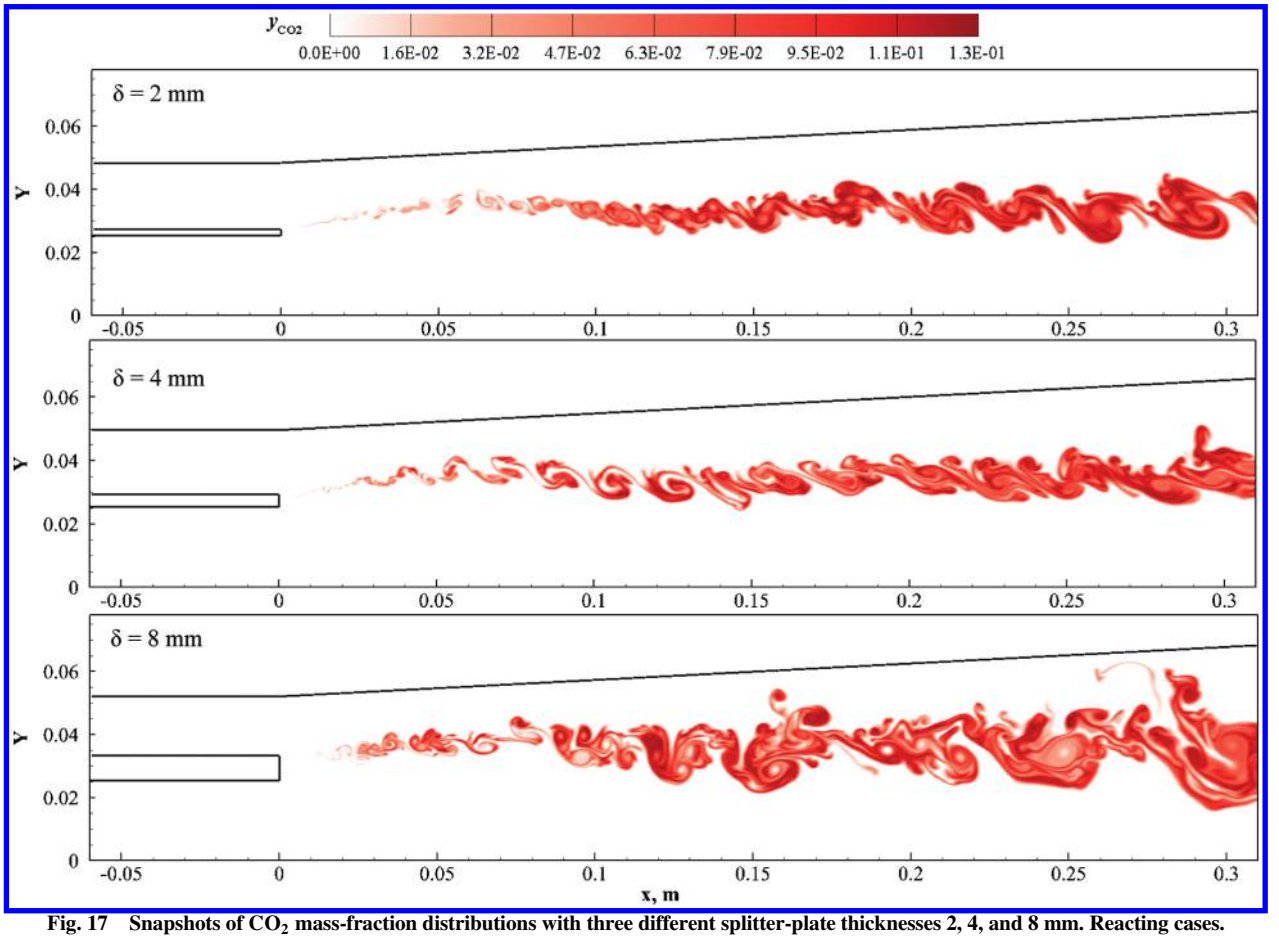

Fig. 17 Snapshots of CO_2 mass-fraction distributions with three different splitter-plate thicknesses 2, 4, and 8 mm. Reacting cases.

ature. For all three cases, only limited amounts of CO_2 production were observed in the recirculation zone.

2. *Flow and Flame Characteristics in Near Field*

Flow characteristics in the near field were examined to help identify the flame-holding mechanism and spreading behaviors. Figure 18 shows instantaneous distributions of the pressure and density, their gradients, and velocities with the splitter-plate thickness of 4 mm. As the isolator airflow and the gas-generator hot stream entered the supersonic combustor, two expansion fans emanated immediately from the inner and outer edges of the splitter plate, reducing the near-rim pressure and density to less than 20 kPa and 0.10 kg/m^3, respectively. Flow overexpansions then induced oblique shocks, a peculiar phenomenon in a supersonic environment. The inner and outer flows, which ran toward each other in the expansion zones, were subsequently diverted, as suggested by the curved isolines in the radial-velocity contour. A mixing layer formed between the two oblique shocks, tilted toward the outer airstream with a lower initial density. These shock-induced flow diversions delayed the mixing-layer development, due to attenuated entrainment. A strong reversed flow was created near the splitter plate, with an axial velocity less than −500 m/s along the mixing layer.

Figure 19 shows the distributions of the corresponding temperature, Mach number, mixture fraction, and vorticity. Note that sonic points are connected by dashed lines on the Mach-number contour; isolines of CO_2 mass fraction are plotted on the mixture-fraction contour; and velocity vectors are presented on the vorticity contour. Shear layers originating from the splitter-plate inner and outer edges merged at an axial location of 2.5 mm. From this point on, combustion products, such as CO_2, began to accumulate and exceeded a value of 0.001. A narrow supersonic region was attached to the rear rim as a result of reversed flows. Although a proper mixture fraction was present in this region, combustion did not take place, due to an insufficient flow residence time. Outside the thin supersonic strip, the mixture fraction was not appropriate to support chemical reactions in the recirculation zone.

The oxidation studies of ethylene/air mixtures by Kopp et al. [31,32] suggest that the ignition time delay at a temperature of 1300 K is less than 50 μs for equivalence ratios of 0.3 and 0.5 and around 100 μs for stoichiometric mixtures. It decreases with increasing

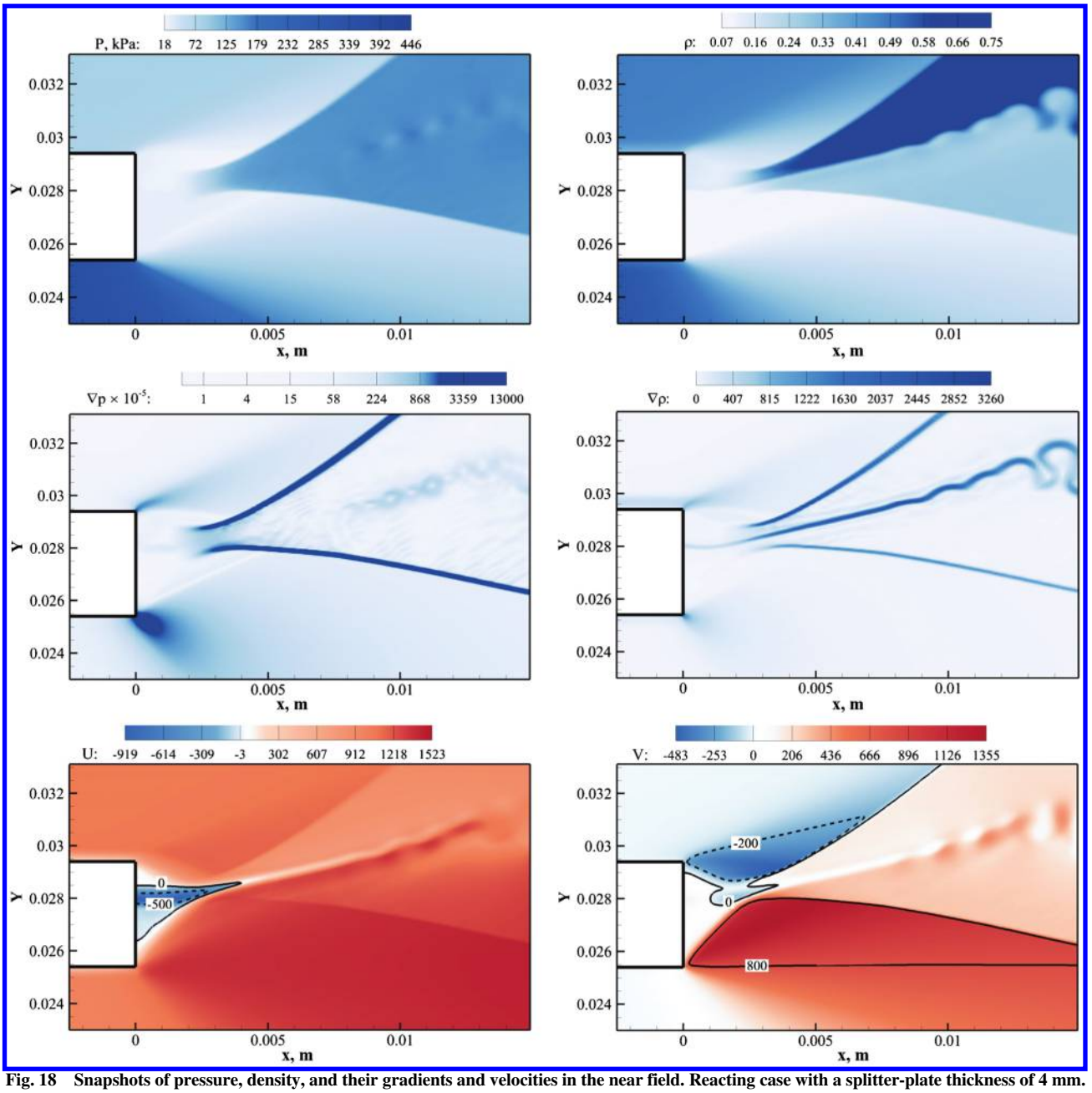

Fig. 18 Snapshots of pressure, density, and their gradients and velocities in the near field. Reacting case with a splitter-plate thickness of 4 mm.

Downloaded by GEORGIA INST OF TECHNOLOGY on September 7, 2015 | http://arc.aiaa.org | DOI: 10.2514/1.B35740

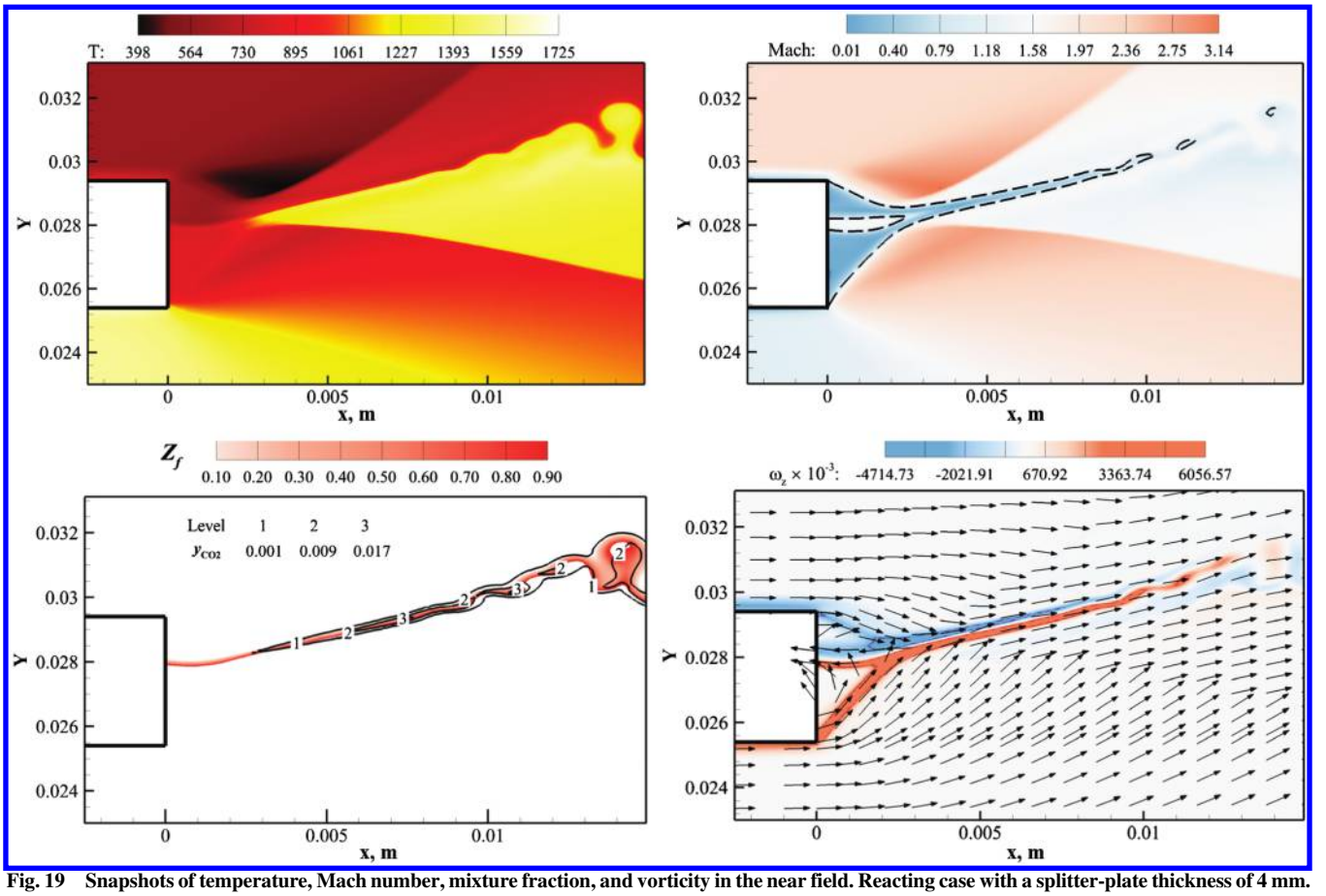

Fig. 19 Snapshots of temperature, Mach number, mixture fraction, and vorticity in the near field. Reacting case with a splitter-plate thickness of 4 mm.

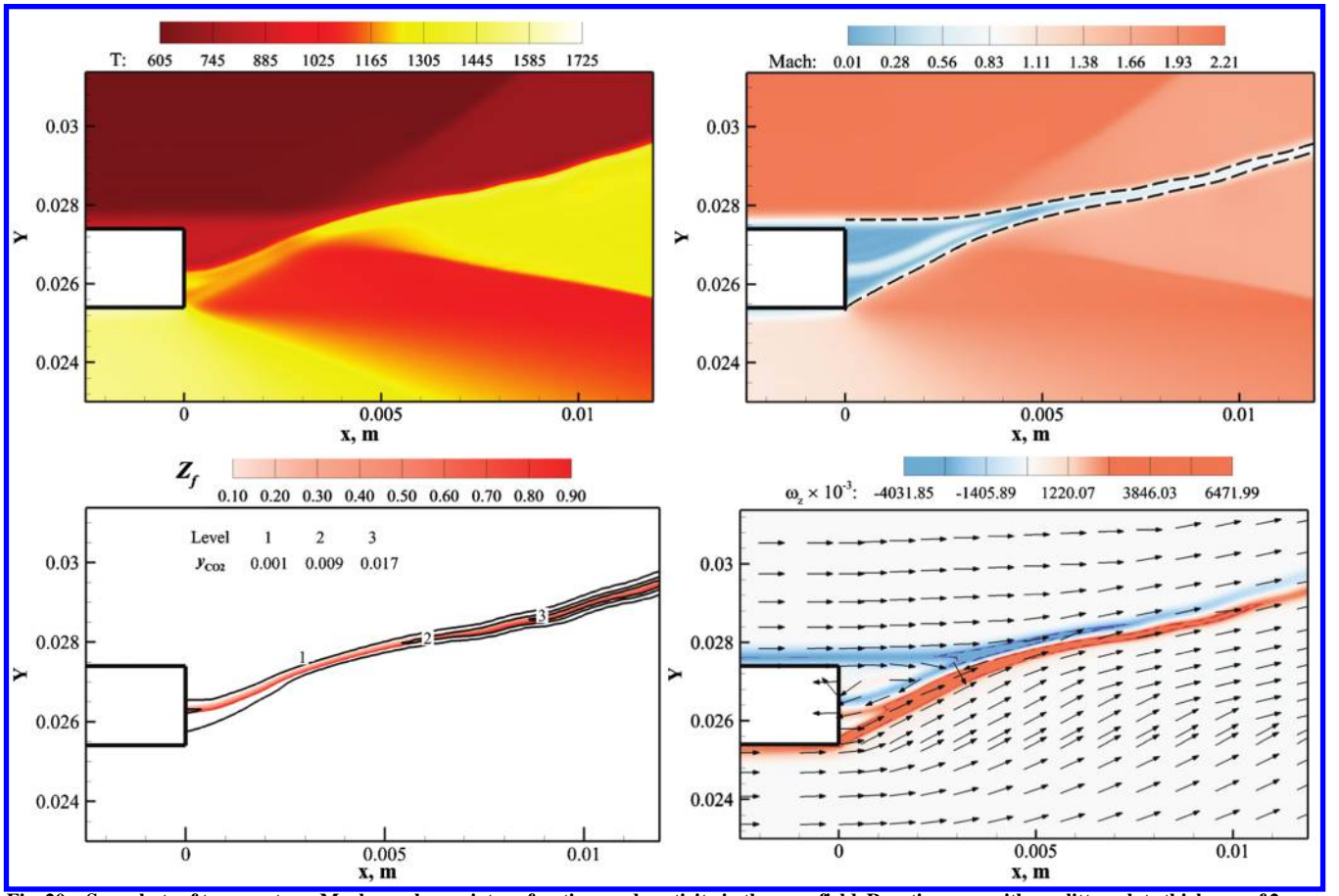

Fig. 20 Snapshots of temperature, Mach number, mixture fraction, and vorticity in the near field. Reacting case with a splitter-plate thickness of 2 mm.

Downloaded by GEORGIA INST OF TECHNOLOGY on September 7, 2015 | http://arc.aiaa.org | DOI: 10.2514/1.B35740

temperatures. Since ethylene oxidation in the gas generator produces a mixture rich in free radicals with a flame temperature over 1600 K, the ignition time delay is largely reduced. Autoignition is expected, so long as a proper mixture is formed in the region with a moderate flow residence.

Figure 20 shows instantaneous distributions of the temperature, Mach number, mixture fraction, and vorticity with a splitter-plate thickness of 2 mm. Compared to Fig. 19, the near-field recirculation zone shrank but remains subsonic. CO_2 was detected, indicating the existence of an attached flame. This phenomenon may be attributed to the fact that, as the splitter-plate thickness decreased, the expansions of the two incoming streams weakened. With a velocity on the order of 10 m/s and a characteristic length being the plate thickness of 2 mm, the flow residence time in the subsonic region was on the order of 100 μs. A combustion-favorable environment was created in the splitter-plate wake flow, and autoignition occurred once the mixture fraction fell in the flammability region.

Figure 21 shows snapshots of the temperature, Mach number, mixture fraction, and vorticity fields with a splitter-plate thickness of 8 mm. Such a geometry change caused strong flow expansion and unsteadiness. The resultant stretching in the near-field mixing layer prohibited any chemical reactions. Immediately downstream of the splitter plate, a proper mixture fraction was not correlated with the low-speed flow; in other regions in which the flow speed was sufficiently low, mixing was not well established, and the flame was detached from the rim.

In all, the recirculating wake flow behind the splitter plate was crucial in determining the mixing behaviors of the coflow fuel and air. It was not, however, sufficient to stabilize the flame in the present study. Its size and shape were strongly affected by splitter-plate thickness, due to rapid flow expansion under supersonic conditions. Significant flow mixing and associated dynamics commenced downstream of the wake region. Depending on the local mixing and flow properties, autoignition occurred either in the wake flow or at some distance downstream of the mixing layer. For the former, the flame appeared to be stabilized by the recirculation zone. In the latter case, a lifted flame occurred and was intermittently connected to the wake through thin reacting filaments. Sporadic autoignition occurred in the later mixing layer to sustain stable combustion in the system.

IV. Conclusions

Supersonic flow and flame characteristics were numerically investigated for an ethylene and air coflow with a splitter plate in a dual-combustion ramjet engine environment. Various flow and combustion phenomena were explored with three different splitter-plate thicknesses of 2, 4, and 8 mm. Special attention was given to flame stabilization immediately downstream of the splitter plate and the ensuing spreading process in the mixing layer.

Analysis was first performed for nonreacting cases. The stream from the gas generator behaves as an underexpanded supersonic jet as it enters the wall-confined supersonic combustor, inducing a series of complex flow structures, including expansion and compression shock waves, boundary-layer separation, and reattachment. In the near field, a recirculation zone occurs downstream of the splitter plate along with two oblique shocks stemming from the plate edges. Further downstream, a supersonic mixing layer forms between the two oblique shocks, and its development is influenced by the discontinuities that are intrinsic to supersonic environments.

The combustion cases were treated using a laminar chemistry model. The overall reacting flowfield bears close resemblance to its nonreacting counterpart, except for moderate suppression of the mixing-layer development due to heat release. The reaction zone starts downstream of the splitter plate and spreads over the entire mixing layer. The spatial location of ignition is dictated by local flow expansion and mixing effectiveness. For a thin splitter plate, the flame is attached, whereas lifted flames are observed for thicker plates, a phenomenon that can be attributed to the strong flow expansion with increasing plate thickness. On the other hand, as the splitter plate thickens, mixing dynamics is enhanced, leading to more complete combustion.

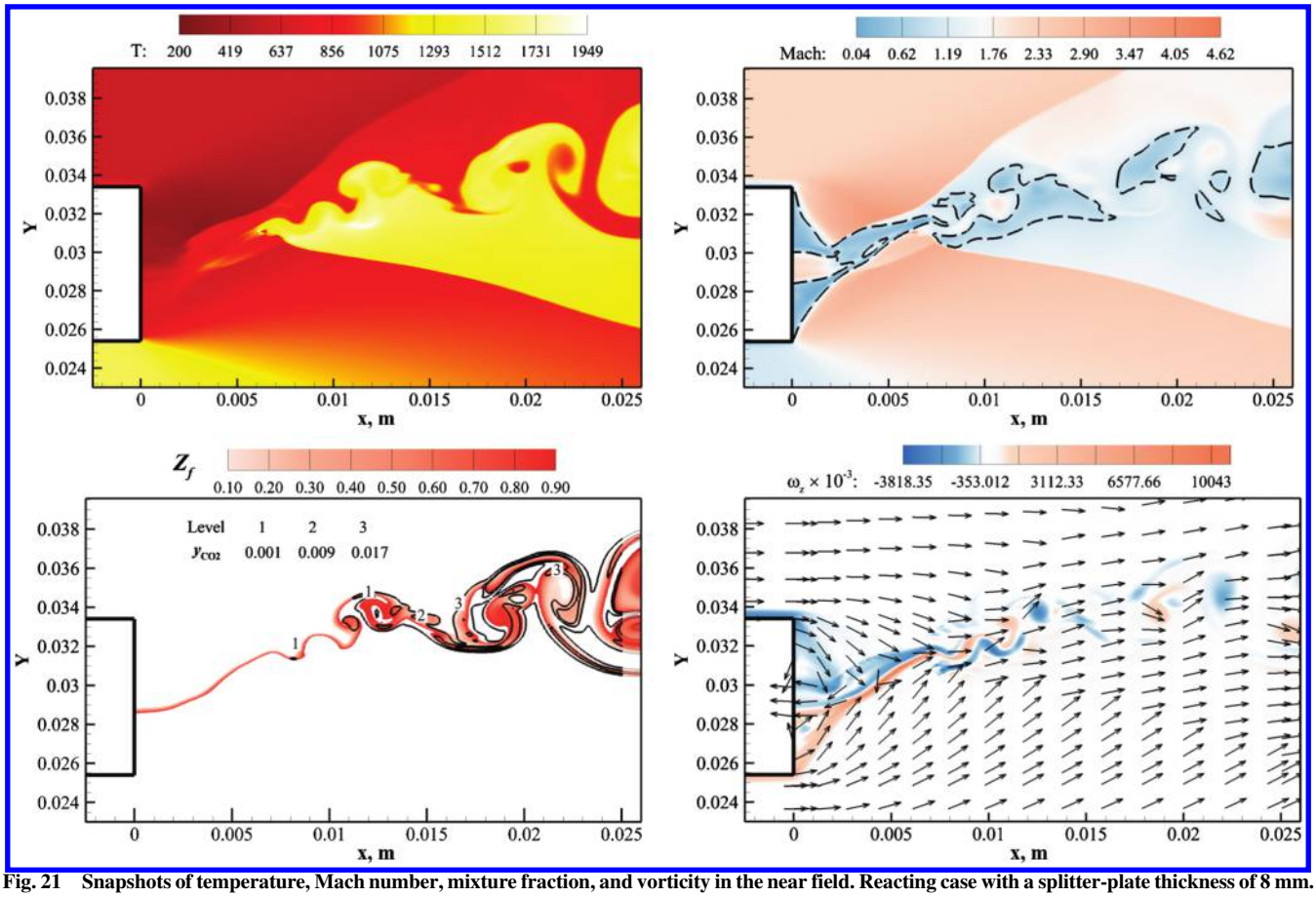

Fig. 21 Snapshots of temperature, Mach number, mixture fraction, and vorticity in the near field. Reacting case with a splitter-plate thickness of 8 mm.

Downloaded by GEORGIA INST OF TECHNOLOGY on September 7, 2015 | http://arc.aiaa.org | DOI: 10.2514/1.B35740

Acknowledgments

This work was sponsored by the William R. T. Oakes Endowment at the Daniel Guggenheim School of Aerospace Engineering at the Georgia Institute of Technology.

References

[1] Curran, E. T., "Scramjet Engines: The First Forty Years," *Journal of Propulsion and Power*, Vol. 17, No. 6, 2001, pp. 1138–1148. doi:10.2514/2.5875

[2] Waltrup, P. J., White, M. E., Zarlingo, F., and Gravlin, E. S., "History of U.S. Navy Ramjet, Scramjet, and Mixed-Cycle Propulsion Development," *Journal of Propulsion and Power*, Vol. 18, No. 1, 2002, pp. 14–27. doi:10.2514/2.5928

[3] Fry, R. S., "A Century of Ramjet Propulsion Technology Evolution," *Journal of Propulsion and Power*, Vol. 20, No. 1, 2004, pp. 27–58. doi:10.2514/1.9178

[4] Segal, C., *The Scramjet Engine: Processes and Characteristics*, Cambridge Univ. Press, New York, 2009.

[5] Billig, F. S., Waltrup, P. J., and Stockbridge, R. D., "Integral-Rocket Dual Combustion Ramjets: A New Propulsion Concept," *Journal of Spacecraft*, Vol. 17, No. 5, 1980, pp. 416–424. doi:10.2514/3.57760

[6] Billig, F. S., "Supersonic Combustion Ramjet Missile," *Journal of Propulsion and Power*, Vol. 11, No. 6, 1995, pp. 1139–1146. doi:10.2514/3.23952

[7] Waltrup, P. J., "Liquid-Fueled Supersonic Combustion Ramjets: A Research Perspective," *Journal of Propulsion and Power*, Vol. 3, No. 6, 1987, pp. 515–524. doi:10.2514/3.23019

[8] Colket, M. B., III, and Spadaccini, L. J., "Scamjet Fuels Autoignition Study," *Journal of Propulsion and Power*, Vol. 17, No. 2, 2001, pp. 315–323. doi:10.2514/2.5744

[9] Puri, P., Ma, F.-H., Choi, J.-Y., and Yang, V., "Ignition Characteristics of Cracked JP-7 Fuel," *Combustion and Flame*, Vol. 142, No. 4, 2005, pp. 454–457. doi:10.1016/j.combustflame.2005.06.001

[10] Papamoschou, D., and Roshko, A., "The Compressible Turbulent Shear Layer: An Experimental Study," *Journal of Fluid Mechanics*, Vol. 197, No. 1, 1988, pp. 453–477. doi:10.1017/S0022112088003325

[11] Dimotakis, P. E., "Turbulent Free Shear Layer Mixing and Combustion," *High Speed Propulsion Systems*, edited by Murthy, S. N. B., and Curran, E. T., Vol. 137, Progress in Astronautics and Aeronautics, AIAA, Washingdon, D.C., 1991, pp. 265–340.

[12] Clemens, N. T., and Mungal, M. G., "Large-Scale Structure and Entrainment in the Supersonic Mixing Layer," *Journal of Fluid Mechanics*, Vol. 284, No. 1, 1995, pp. 171–216. doi:10.1017/S0022112095000310

[13] Fernández-Tarrazo, E., Vera, M., and Liñánc, A., "Liftoff and Blowoff of a Diffusion Flame Between Parallel Streams of Fuel and Air," *Combustion and Flame*, Vol. 144, Nos. 1–2, 2006, pp. 261–276. doi:10.1016/j.combustflame.2005.07.012

[14] Kurdyumov, V., and Matalon, M., "Stabilization and Onset of Oscillation of an Edge-Flame in the Near-Wake of a Fuel Injector," *Proceedings of the Combustion Institute*, Vol. 31, No. 1, 2007, pp. 909–917. doi:10.1016/j.proci.2006.07.248

[15] Clemens, N., and Mungal, M., "Two- and Three-Dimensional Effects in the Supersonic Mixing Layer," *AIAA Journal*, Vol. 30, No. 4, 1992, pp. 973–981. doi:10.2514/3.11016

[16] Yu, K. H., Parr, T. P., and Schadow, K. C., "Planar Mie Scattering Visualization of Reacting and Nonreacting Supersonic Coaxial Jets," *International Journal of Energetic Materials and Chemical Propulsion*, Vol. 3, Nos. 1–6, 1994, pp. 504–517. doi:10.1615/IntJEnergeticMaterialsChemProp.v3.i1-6.520

[17] Otakeyama, Y., Takeshi Yokomori, T., and Mizomoto, M., "Stability of $CH_4 - N_2$/Air Jet Diffusion Fame for Various Burner Rim Thicknesses," *Proceedings of the Combustion Institute*, Vol. 32, No. 1, 2009, pp. 1091–1097. doi:10.1016/j.proci.2008.05.002

[18] Menter, F. R., "Two-Equation Eddy-Viscosity Turbulence Models for Engineering Applications," *AIAA Journal*, Vol. 32, No. 8, 1994, pp. 1598–1605. doi:10.2514/3.12149

[19] Spalart, P. R., Jou, W.-H., Strelets, M., and Allmaras, S. R., "Comments on the Feasibility of LES for Wings, and on a Hybrid RANS/LES Approach," *Advances in DNS/LES*, Greyden Press, Columbus, OH 1997, pp. 137–148.

[20] Strelets, M., "Detached Eddy Simulation of Massively Separated Flows," AIAA Paper 2001-0879, 2001.

[21] Choi, J. Y., Jeung, I. S., and Yoon, Y., "Numerical Study of Scram Accelerator Starting Characteristics," *AIAA Journal*, Vol. 36, No. 6, 1998, pp. 1029–1038. doi:10.2514/2.476

[22] Singh, D. J., and Jachimowski, C. J., "Quasi-Global Reaction Model for Ethylene Combustion," *AIAA Journal*, Vol. 32, No. 1, 1994, pp. 213–216. doi:10.2514/3.11972

[23] Jachimowski, C. J., "An Experimental and Analytical Study of Acetylene and Ethylene Oxidation Behind Shock Waves," *Combustion and Flame*, Vol. 29, No. 1, 1977, pp. 55–66. doi:10.1016/0010-2180(77)90093-1

[24] Evans, J. S., Schexnayder, C. J., Jr., and Beach, H. L., Jr., "Application of a Two-Dimensional Parabolic Computer Program to Prediction of Turbulent Reacting Flows," NASA TP-1169, 1978.

[25] Evans, J. S., and Schexnayder, C. J., "Influence of Chemical Kinetics and Unmixedness on Burning in Supersonic Hydrogen Flames," *AIAA Journal*, Vol. 18, No. 2, 1980, pp. 188–193. doi:10.2514/3.50747

[26] Möbus, H., Gerlinger, P., and Brüggermann, D., "Scalar and Joint Scalar-Velocity-Frequency Monte Carlo PDF Simulation of Supersonic Combustion," *Combustion and Flame*, Vol. 132, Nos. 1–2, 2003, pp. 3–24. doi:10.1016/S0010-2180(02)00428-5

[27] Koo, H., Donde, P., and Raman, V., "A Quadrature-Based LES/Transported Probability Density Function Approach for Modeling Supersonic Combustion," *Proceedings of the Combustion Institute*, Vol. 33, No. 2, 2011, pp. 2203–2210. doi:10.1016/j.proci.2010.07.058

[28] Li, J., Zhang, L., Choi, J.-Y., Yang, V., and Lin, K. C., "Ignition Transients in a Scramjet Engine with Air Throttling, Part 1: Nonreacting Flow," *Journal of Propulsion and Power*, Vol. 30, No. 2, 2014, pp. 438–448. doi:10.2514/1.B34763

[29] Li, J., Zhang, L., Choi, J.-Y., Yang, V., and Lin, K. C., "Ignition Transients in a Scramjet Engine with Air Throttling Part II: Reacting Flow," *Journal of Propulsion and Power*, Vol. 31, No. 1, 2015, pp. 79–88. doi:10.2514/1.B35269

[30] Ashkenas, H., and Sherman, F. S., "The Structure and Utilization of Supersonic Free Jets in Low Density Wind Tunnels," *Rarefied Gas Dynamics Volume II*, Academic Press, New York, 1966, pp. 84–105.

[31] Kopp, M. M., Donato, N. S., Petersen, E. L., Metcalfe, W. K., Burke, S. M., and Curran, H. J., "Oxidation of Ethylene-Air Mixtures at Elevated Pressures, Part 1: Experimental Results," *Journal of Propulsion and Power*, Vol. 30, No. 3, 2014, pp. 790–798. doi:10.2514/1.B34890

[32] Kopp, M. M., Petersen, E. L., Metcalfe, W. K., Burke, S. M., and Curran, H. J., "Oxidation of Ethylene-Air Mixtures at Elevated Pressures, Part 2: Chemical Kinetics," *Journal of Propulsion and Power*, Vol. 30, No. 3, 2014, pp. 799–811. doi:10.2514/1.B34891

C. Segal
Associate Editor

Downloaded by GEORGIA INST OF TECHNOLOGY on September 7, 2015 | http://arc.aiaa.org | DOI: 10.2514/1.B35740